Review TRENDS in Cell Biology Vol.xx No.xx Monthxxxx

New views of cells in 3D: an introduction to electron tomography

Richard McIntosh, Daniela Nicastro and David Mastronarde

Laboratory for 3D Electron Microscopy of Cells, Department of Molecular, Cellular and Developmental Biology, University of Colorado, Boulder, CO 80309-0347, USA

The most important goal of structural cell biology is to elucidate the mechanisms of the processes of life. The structure of a membrane system or fibrous array, the changes in such structures over time or the localizations of enzymes relative to organelle boundaries can often illuminate associated cellular functions. To be of maximal value, structural studies should provide isotropic, 3D information about well-preserved samples at the highest possible resolution. Electron tomography can provide such information about many kinds of cells and organelles.

Introduction

Electron microscopic tomography (ET) produces 3D images of cells that show macromolecular assemblies such as membranes, fibers and multi-enzyme complexes in the contexts in which they normally function. The resolution of such images currently ranges from 3 to 8 nm and provides valuable information about the structural basis of many cellular processes.

In this review, we provide an introduction to ET and several illustrations of the method, showing its power for characterizing subcellular architecture and structural detail. We also discuss ways in which ET can be integrated with other methods, such as single-particle averaging, to extend its resolution. We highlight the strengths and limitations of the method, focusing on techniques that can identify and localize specific macromolecules in tomograms, because such techniques greatly enrich the information that can be gleaned from structural studies.

What is ET?

Electron tomography is a method for generating 3D images on the basis of multiple 2D projection images of a 3D object, obtained over a wide range of viewing directions (Figure 1a,c,d). The sought-after 3D image is generated in a computer by back-projecting each 2D image with appropriate weighting [1,2] (Figure 1b,d,e; see also Supplementary Videos 1,2,3). ET is analogous to the various tomographies used in modern medicine that are based on X-rays, the γ-rays produced by positron annihilation, magnetic resonance or ultrasound; however, the high resolution of electron microscopy (EM) facilitates 3D reconstructions that reveal not only long-range cellular features, such as the trajectories of cytoskeletal fibers [3,4], but also the details of organelle structure at a level that approaches macromolecular dimensions [5]. As a result, ET provides highly informative images of functionally significant cellular structures. Compared with scanning confocal fluorescence and deconvolution light microscopy, ET offers an improvement in resolution of 40–100-fold. This improvement comes, however, at a considerable cost in terms of effort and financial expense. Moreover, although ET can readily produce a snapshot of a cell in 3D, following time-dependent events by ET requires the assembly of images from several samples.

A tomogram is a 3D block of data that is represented as an array of volume elements (voxels). The voxels are typically cubes 1–4 nm per side, each with a grayscale value that corresponds to the mass density in that region of the specimen. Because macromolecules are slightly denser than their aqueous solvent, they interact more strongly than their background with electrons in the beam of the microscope – a process called 'electron scattering'. Because this scattering depends strongly on the atomic numbers of the molecules involved, it can be enhanced by staining macromolecules with heavy metals. In this case, however, the scattering results predominantly from the stain, so the information about macromolecule structure and position is derived indirectly.

The resulting reconstructions can be viewed in planes displayed as 2D images at selected values of the third dimension. Examples of such tomographic slices are shown in Figure 2a,c,f; these images look like conventional electron micrographs, but they differ in two important ways. First, each image shows a slice that is only a few nanometers thick, defined by the size of the voxels in the reconstruction; thus, the wafer of biological material viewed is far thinner than can be cut with an ultramicrotome and diamond knife. This means that the resolution in the dimension along the axis of view is almost as good as the resolution in the image itself. Second, each image displays only one slice from the many that comprise the reconstruction; therefore, the structure and position of complex features can be determined by examining neighboring slices. As an example, Figure 2a shows three slices from a flagellar basal body in *Chlamydomonas*. These slices show that the ninefold star located in the region of transition from basal body to axoneme is actually composed of two stars separated by an unstructured zone with a thickness of about 5 nm (arrow) [6]. This

Corresponding author: McIntosh, R. (richard.mcintosh@colorado.edu).

 0962-8924/$ - see front matter doi:10.1016/j.tcb.2004.11.009

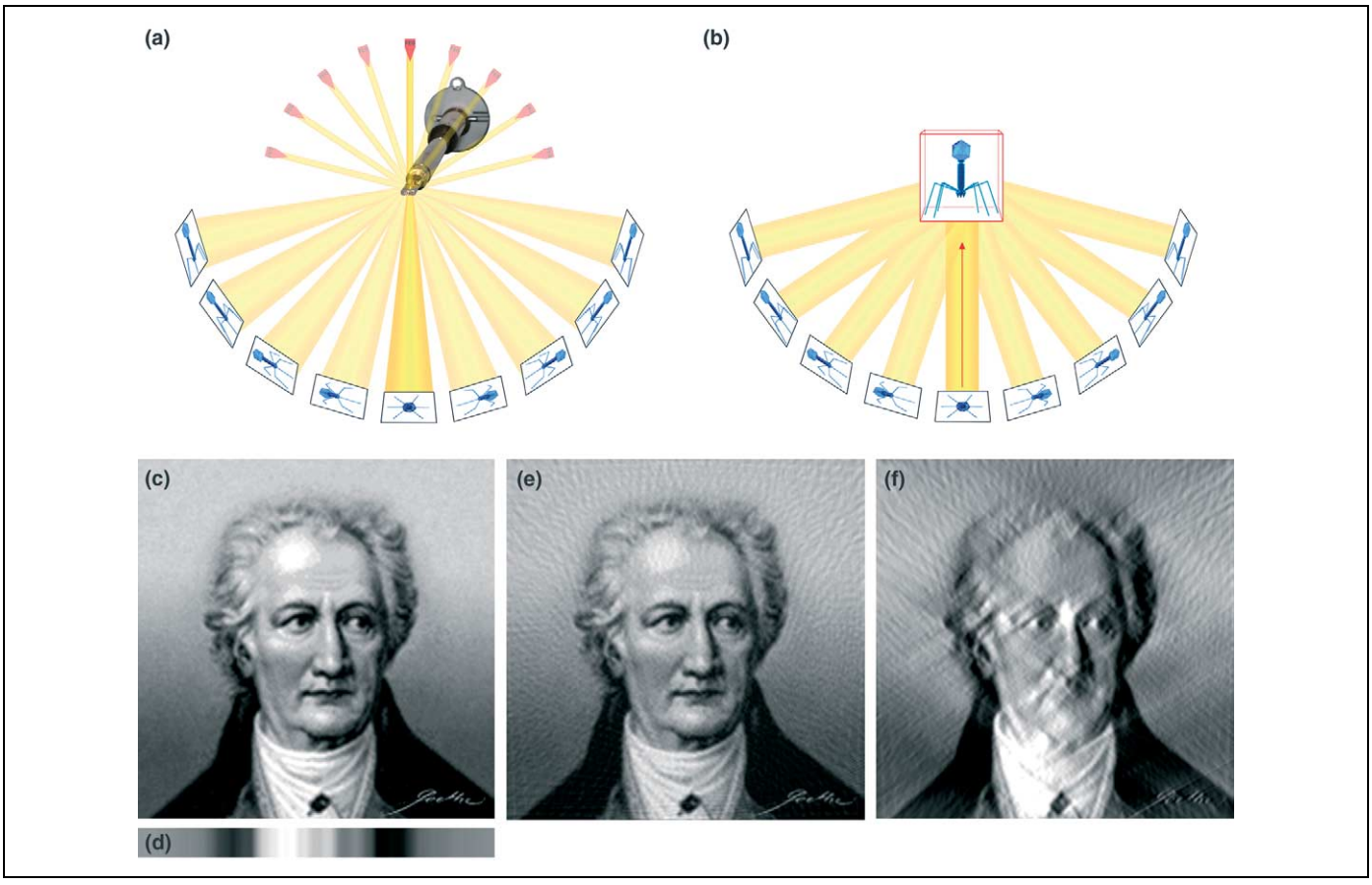

Figure 1. Principles of ET. **(a)** A biological specimen, in this case a bacteriophage contained in an EM sample holder, can be imaged from several orientations by tilting the holder in the microscope. **(b)** Process of computed back-projection, in which each tilted view is used to contribute to a reconstruction of the original structure. **(c)** Example of a 2D image (the face of Goethe), representing a slice cut from a 3D object in a plane perpendicular to the tilt axis. **(d)** Projection of the 2D object as a 1D distribution of densities reflecting the summation of all of the brightness in the picture along a set of vertical lines. **(e)** Reconstruction of Goethe's face achieved by back-projecting 90 of the 1D projections taken at 2° intervals between +90° and −90° from the horizontal. The ripples in the image represent the resolution limitation caused by having only 90 images. Twice the number of images taken at half the tilt increment would reduce the size of the ripples by approximately twofold. **(f)** A further limitation on resolution is imposed by reconstructing the image from a more restricted range of tilted views taken between +60° and −60° from the horizontal. Because a wedge of data is missing, the reconstruction quality is anisotropically degraded. The vertical detail is still sharp (note the clarity of the shoulders, the nose and the ear); by contrast, the horizontal detail is poorly defined (note the virtual absence of a mouth). This kind of anisotropy is characteristic of single-axis tomograms constructed from data collected from a limited range of tilt.

feature of the transition zone had previously escaped notice, even though basal bodies had been studied by EM for years.

The visualization of complex structures can be facilitated by representing them with graphic models. If the contrast is good and the background is sparse, boundaries around features of interest can be identified automatically, simply by choosing an appropriate threshold in the distribution of 3D density. For example, γ-tubulin ring complexes, with and without attached microtubules, have been reconstructed by ET, providing both the context to identify the complexes and the resolution to see their organization [7] (Figure 2b). Automated detection of structures is often facilitated by prior image filtering, which can reduce the background fluctuations, or 'noise', in the image and, thereby, increase the signal-to-noise ratio. This process is currently receiving considerable attention from the mathematical community [8].

Another way in which to model tomographic features of interest is to trace them by hand, marking their contours on many successive slices in 3D. Such contours can be used with classic methods of computer graphics to fit a surface in space, light it appropriately and view it as a 3D representation. Figure 2c shows a slice from a reconstruction of an axon at a node of Ranvier, and Figure 2d is the model generated from contours drawn on several such tomographic slices. Color has been applied by the investigator to indicate objects with distinct biological functions [9]. The full value of such a color model is best seen when the graphic is rotated in space and shown as a movie (a further example is shown in Supplementary Video 4). Manual contouring on many tomographic slices is, however, time-consuming. Fortunately, mathematical methods for automating this type of feature recognition are under development in several laboratories, which should soon speed up this kind of work [8,10].

Both tomograms and models can be zoomed, panned, tilted and rotated for easy viewing and can be used for quantitative structural analysis. For example, Figure 2e shows unprecedented detail from a phragmoplast, the organelle that achieves cytokinesis in a plant cell. The microtubules, the vesicles that accumulate in the midzone of the cell, the tubular organelles that form from the fusion of these vesicles, and the elements of the forming cell plate, in addition to the spaces between them, can be clearly seen and measured. The lengths, areas and

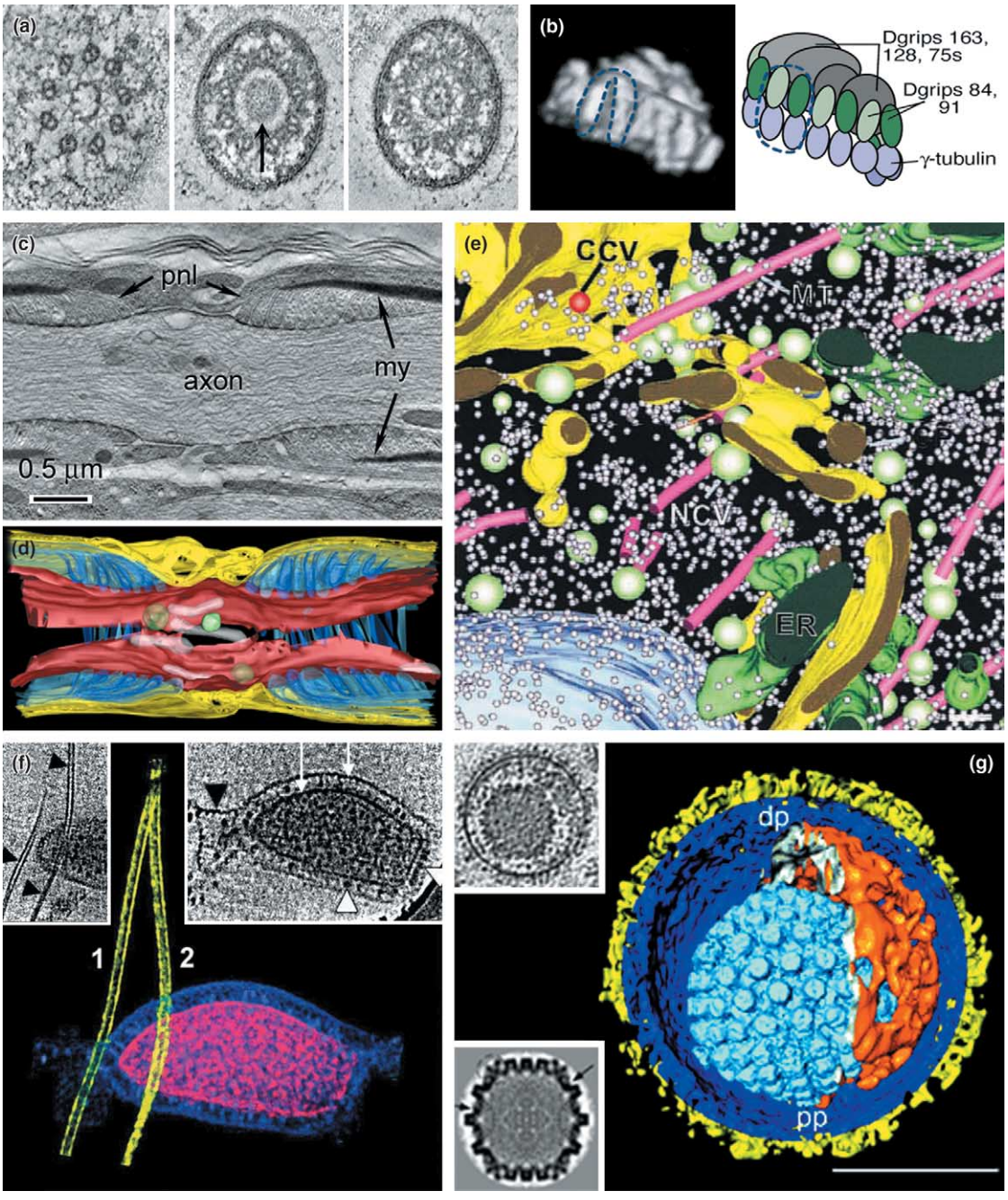

Figure 2. Tomograms and 3D models of biological structures. **(a)** Slices (each ~1.5-nm thick) from a tomogram of a basal body from *Chlamydomonas reinhardtii*. The two-layered arrangement of the material in the ninefold star is apparent from the middle slice, which lacks the star (arrow). Images reproduced, with permission, from Ref. [6]. **(b)** A 3D reconstruction of the γ-tubulin ring complex, viewed as shaded surfaces identified by a grayscale threshold (left) and as a model (right) in which the molecular components are identified. Images reproduced, with permission, from Ref. [7]. **(c)** Slice from a tomogram of a node of Ranvier, showing the axon, the myelin sheath (my) and the paranodal loops (pnl). Scale bar=0.5 μm. **(d)** Features of the node of Ranvier shown in a 3D model based on many tomographic slices such as those shown in (c). The volume comprises a thickness of approximately 1.5 μm and an area of approximately 2×5 μm. The axolemma (red), paranodal loops (blue), mitochondria (white) and intra-axonal vesicles (green) are indicated. Images in (c,d) reproduced, with permission, from Ref. [9]. **(e)** Model constructed from hand-drawn contours marking the boundaries of cellular components in a tomogram of the phragmoplast formed during pollen development in *Arabidopsis thaliana*. Scale bar=50 nm. Image reproduced, with permission, from Ref. [11]. **(f)** Images of the archaeon *Pyrodictium*. The cell and its associated extracellular fibers, called cannulae (small black arrowheads), are visible in the two tomographic slices (top left and right). The plasma membrane and the S-layer can be seen clearly (white arrows) and there are particles in the periplasmic space (white arrowhead). At one end of the cell, the S-layer bulges (large black arrowhead). The pseudocolored representation shows the cannulae in yellow (labeled 1 and 2), the cytoplasm in magenta, and the periplasm and S-layer in blue. Images reproduced, with permission, from Ref. [49]. **(g)** The virion of *Herpes simplex* virus. Top inset, a 5.2-nm slice from a tomogram showing the envelope (blue and yellow), the protein-containing 'tegument' (orange) within it, and the nucleocapsid (light blue). Bottom inset, results of averaging to improve the image signal-to-noise ratio. Tomography also reveals the pleiomorphic structures surrounding the nucleocapsid, although the signal-to-noise ratio is lower. The pseudocolored representation shows a model of the whole virus based on cryo-ET. Scale bar=100 nm. Images reproduced, with permission, from Ref. [58]. Abbreviations: CCV, clathrin-coated vesicle; CP, cell plate; dp, distal pole; ER, endoplasmic reticulum; MT, microtubule; NCV, non-coated vesicle; pp, proximal pole.

volumes of these components determined in tomograms from different stages in cytokinesis have led to the tentative identification and placement of macromolecules such as dynamin that deform membranes in well-defined ways [11,12]. Thus, tomography can help cell biologists to analyze and to understand diverse structures of mechanistic interest.

ET of different types of specimen

As in all types of microscopy, the quality of the specimen limits the quality of the final image. ET was first applied to cellular samples prepared by conventional methods, including chemical fixation, dehydration and embedding [13–16]. These results were informative about medium-to-large scale features such as chromatin organization, but their details were subject to the concern that is commonly leveled at EM: namely, fixation artifacts.

More recently, tomography has been used to reconstruct EM specimens prepared by 'ultrarapid' freezing [17,18], in which the specimen is plunged into liquid ethane to drop its temperature at a rate of about 10^4 °C/s [19]. Such preparations are likely to represent living cells accurately because the sample is frozen within milliseconds and because many of the cells that are frozen in this way will grow and divide when warmed rapidly to physiological temperatures [20]. Thus, they merit careful study at high resolutions. Well-frozen cells can be either examined directly in the EM, by using a cold stage that maintains a temperature of less than −160 °C (cryo-EM), or dehydrated, fixed and embedded at low temperatures by 'freeze substitution'.

The craft of rapid freezing

The principal problem in preparing frozen biological samples is freezing them without causing ice crystal damage. Water that is cold enough will crystallize extremely well. When ice crystals form in cells, the cytoplasm is distorted by the expansion that accompanies freezing; biological structures are largely excluded from the ice and are moved along with the advancing liquid–solid interface.

Many approaches have been devised to avoid such damage, the most successful of which is simply to freeze samples quickly. If the temperature drops rapidly enough, there is not enough time for water molecules to diffuse onto a growing crystal surface before they have lost so much kinetic energy that they no longer move appreciably. The result is vitreous (glass-like) ice, a non-crystalline solid that does not impose its structure on the material that it pervades [21]. Cells that are less than a few micrometers thick can be frozen without crystal damage simply by plunging them into liquid ethane, slamming them onto a cold metal block, or spraying them with liquid propane [22]; however, most cells are too thick to freeze well because heat cannot leave the middle of the sample fast enough to enable good freezing there. Without a 'trick' such as a chemical cryoprotectant (e.g. sugar [23], glycerol or dimethyl sulfoxide), ice crystals cause obvious sample distortion. Because chemical cryoprotectants can modify cell structure, however, their use is generally avoided.

Freezing cells and even tissue samples has become much easier with the advent of high-pressure freezing [24]. High hydrostatic pressure works as a physical cryoprotectant because water expands when it freezes. If the pressure is increased quickly and followed immediately by rapid freezing, the potentially damaging effects of high pressure are minimized and, as in ultrarapid freezing, many frozen cells will live after thawing. With high-pressure freezing, samples as large as 500 μm in their minimum dimension can be frozen with structureless ice [25–27]. This means that some embryos, small invertebrates, tissue samples from large organisms [28], and pellets of microorganisms [29] can be vitrified with comparative ease, facilitating their subsequent study by high-quality EM [30,31]. Although there is some risk that high pressure can modify cell structure even in the few milliseconds that separate pressure onset and freezing, these advances have nurtured two successful approaches to cellular tomography.

ET of freeze-substituted samples

An organic solvent, such as acetone, can be cooled to −90° C and used as a solvent for fixatives and stains including glutaraldehyde, tannic acid, uranyl acetate and osmium tetroxide [32,33]. Cold solvent–fixative mixtures will dissolve solidified intracellular water, in addition to some membrane lipids, such that the fixatives and stains can enter cells and react with cellular macromolecules, albeit slowly at the low temperature. This preparative method is commonly called 'rapid-freezing, freeze-substitution fixation' (RF-FSF). If an RF-FSF sample is kept at low temperature and placed in a resin with adequately low viscosity, the resin will gradually replace the organic solvent, where it can be polymerized by ultraviolet light catalysis to form a solid block in which plastic has replaced cellular water. The sample can now be warmed to ambient temperature, and slices appropriate for EM (20–500-nm thick) can be cut in a microtome. The fidelity of this type of sample preservation has been shown to be accurate for many specimens [20,34–36].

Heavy metal stains added during freeze substitution enhance specimen contrast. Plastic embedding enables samples to be serially sectioned. Together, these features enable RF-FSF samples to be used for the 3D reconstruction of comparatively large volumes. Cellular areas as large as 5×5 μm have been visualized as montages, and increased sizes in the third dimension have been obtained by serial ET. Each microscope specimen, however, must be thin enough to enable imaging with good resolution: 200 nm or less in a microscope at 200 keV, 400 nm or less at 300 keV, and 500 nm or less at 1000 keV is required to obtain a resolution of about 5 nm.

A filter that limits the effects of chromatic aberration (which results from electron energy loss through inelastic scattering in thick samples) permits the imaging of thicker samples, but there is a resulting increase in specimen damage by the beam. So far, volumes of about 25 μm^3 have been reconstructed at a resolution of roughly 6 nm by 'stitching' serial tomograms together [37], but this is only a small fraction of most eukaryotic cells; for example, a mammalian liver cells has a volume of

100–200 μm^3. Improvements will be therefore needed to make large cell reconstructions.

The resolution of RF-FSF ET

The resolution of tomograms generated from RF-FSF samples is subject to debate. The electron optical resolution of individual images is usually good. It depends, of course, on the microscope, the thickness of the sample and the quality of the image detector, but detail at 2 nm is not unusual. The resolution of a tomogram depends on many practical factors, however, such as the angle between tilted views [38], the total range of tilt [39], the precision with which the tilted views are aligned before their back-projection [1], the use of images from two as opposed to one tilt axis [40,41], and the electron dose used for all of the images [42].

Equally important, however, is the quality of the specimen itself. Even when fixation and dehydration are carried out at low temperatures, there is still the possibility that cellular structures are altered during sample preparation. Certainly, enzymes no longer function after RF-FSF, which means that their structures at atomic resolution must have been modified. Moreover, the position of the stain might not accurately reflect the shapes of the macromolecules to which it binds. This problem is exacerbated by the electron doses required for ET; these can cause the stain to migrate and to agglomerate, further compromising resolution.

Each of these factors has been thought to limit the resolution of RF-FSF tomograms to 5–6 nm, although recent work claims a roughly twofold improvement on this value for thin samples [43]. It seems likely that the stain in these samples was reconstructed to a resolution of about 3 nm, but it is not yet clear whether this level of detail is an accurate reflection of the underlying protein structure. In addition, the chemistry of embedding plastics is altered by the electron beam, leading to a loss of some mass from the section and an associated collapse of the thickness of the section [44]. Reconstructions are therefore distorted, and the models built from them must be corrected to represent cells accurately. Moreover, cryo-EM of thin sections cut from frozen-hydrated samples has provided images that are not identical to those seen after RF-FSF [45]. Thus, fixation artifacts are still a concern, even though the RF-FSF preparative method is one of the best available.

The value of RF-FSF ET

Despite these limitations, ET of RF-FSF samples is providing important information about cells and organelles (3,4,6,9,11,12,18,29,37,41,43) (Figure 2a,c–e). ET of cells frozen at successive times during a physiological process [3] or during an experimental perturbation [7] can provide deep insight into the underlying biological mechanisms. Similarly, tomograms that compare mutants with their wild-type counterparts can illuminate the function of specific gene products [6]. Interpreting tomograms is not always easy, but in the right experimental context the wealth of detail that they reveal about cell organization and organelle structure is highly informative.

Cryo-ET

If cells are imaged after rapid freezing while they are embedded simply in solid water (frozen-hydrated), they are likely to be a reliable representation of the living state; in fact, they are probably the most reliable representation that can be examined in a transmission EM. Not only does rapid freezing maintain the viability of some cells in a population, it preserves the structures of proteins to atomic resolution [46]. Nevertheless, cryo-imaging encounters at least two important difficulties of its own.

First, the image contrast is low because it is based on the small differences in mass density between clusters of macromolecules and the frozen cytosol that surrounds them (or more strictly, on the differences in their electron scattering). It is therefore hard to visualize details of cellular substructure. Commonly, an operator will underfocus the objective lens of the microscope to produce a kind of phase contrast, although cellular details are hard to see even with this trick. Second, frozen-hydrated samples are especially sensitive to the electron beam. Ordered arrays of frozen macromolecules have been used to assess the damage done by beam electrons. These studies show that the higher the resolution sought, the lower the dose that is tolerable [47].

The importance of electron dose in cryo-ET

When the electron dose is low enough to preserve information at 1–2 nm ($\sim$2000 electrons/nm^2 at 100 keV), the devices for electron detection that are currently available produce images in which high-resolution information is obscured by 'noise' that results from both limitations in camera performance (e.g. poor detection efficiency for small image details) and the poor electron counting statistics that result from such light exposures. Higher electron doses produce less noisy images, but with 100-keV electrons as little as 10 000 electrons/nm^2 will cause water in the sample to decompose; the hydrogen released will form bubbles of H_2 gas under high pressure [48], severely distorting the sample.

For tomography, the tolerable dose must be divided among the images that are taken at different orientations to provide resolution in the depth of the sample. According to the 'principle of dose fractionation', the signal-to-noise ratio of a tomogram is based on the total dose for all images, not the dose per image; thus, in principle the tolerable dose can be divided among as many pictures as one chooses [42]. In practice, however, the dose per tilted view must be sufficient to produce pictures with enough detail to enable their accurate alignment for back-projection. The restrictions on total dose, the limitations imposed by imaging devices now available, and the intrinsically low contrast of the samples therefore result in noise levels that obscure the fine details in a cryotomogram.

The resolution of cryo-ET

All of this means that although the electron optical resolution in a cryoimage might be excellent, the resolution with which one can reconstruct organelles is currently more limited, being in the region of 5–8 nm

depending on sample thickness, the hardiness of the sample to the beam, and many of the above-mentioned factors that limit the resolution of RF-FSF tomography.

Figure 2f shows a frozen-hydrated archaeon, *Pyrodictium*, that is associated with two extracellular fibers. The insets show different slices through the reconstruction, and the colored figure is a model of the same cell generated by masking out selected structures and rendering their surfaces with different colors [49]. The cellular detail is impressive, but at this resolution even fairly large macromolecules fail to show their characteristic shapes.

Limitations on sample thickness

Higher resolution can be achieved with existing equipment, but it requires samples that are thin. With the thick samples that take advantage of ET, the likelihood that beam electrons will interact more than once with the sample is increased. These 'multiple scattering events' reduce image quality, because the image is no longer a simple projection of the sample and because at least one of the scattering events is likely to have been 'inelastic'. Inelastic scattering does not enhance contrast in cryo-images for several reasons: it does not produce the shift in electron phase that is necessary to form defocus-dependent phase contrast through interference with unscattered electrons; it transfers energy to the sample, causing damage that reduces image quality; and it changes the energy of the electron, resulting in chromatic aberration.

The resulting constraints on specimen thickness apply even when the microscope is equipped with a filter that can remove beam electrons that have lost energy, in part because the number of electrons that have not lost energy becomes so small that problems with counting statistics get worse. Only the smallest cells [49], the thinnest parts of cells [50] and some isolated organelles [51–53] are appropriate for cryo-ET without the companion use of a process that cuts the frozen-hydrated sample into slices of suitable thickness.

Sectioning vitrified, frozen-hydrated samples has proved to be difficult [54–56]. It is significantly harder than the cryosectioning commonly used for immuno-EM, in which specimens are chemically fixed, impregnated with sucrose as a cryoprotectant, and then frozen for sectioning before being warmed to room temperature and stained with labeled antibodies [57]. Most cryo-ET has therefore focused on samples that are naturally thin. At present, the number of biologically and medically important samples that cannot be reconstructed by this method is vast. Indeed, all tissue samples, most cultured metazoan or plant cells, and even isolated chloroplasts are too thick for cryo-ET at a resolution of <10 nm. Interest is now intense in developing methods for cutting good sections from rapidly frozen samples so that a broader range of samples can be explored with this promising technique [45].

Ways to improve the information available from ET

Improving resolution by image averaging

Even with existing specimens and equipment, there are ways to improve the resolution of cryo-ET and thus the quality of the information that it produces. If the sample contains many identical copies of a given structure, their images can be averaged such that tomograms based on a low electron dose (poor counting statistics) can be made to yield information with a higher signal-to-noise ratio.

Figure 2g shows an application of this approach to cryo-ET of *Herpes simplex* virus. A slice from a tomogram of the whole virion shows the outer envelope, the inner nuclear capsid, and the 'tegument' that lies between (Figure 2g, top inset). The capsids are symmetric and comparatively regular, which means that images from several identical particles can be averaged to improve the signal-to-noise ratio and to increase the resolution (Figure 2g, bottom inset). The authors estimated an improvement in resolution from worse than 7.2 nm for individual tomograms to about 5.6 nm when all of the symmetrically placed subunits from ten capsids were averaged [58]. The colored figure assembles information from both the averaged images and the pleiomorphic material that surrounds the capsid (Figure 2g).

In studies using more extensive averaging, cryotomograms are already yielding information at a resolution of about 4 nm [17,59]. It should be noted, however, that the useful averaging of multiple images requires the structures to be truly identical and not in a multiplicity of functional states. In addition, individual particles must be imaged well enough to permit an accurate 3D alignment with others.

Identification and localization of cellular components

If the resolution in cryo-ET can be improved, many macromolecules should become identifiable and thus localizable in a cell. With current techniques, vesicles prepared from mitochondrial inner membrane have shown membrane-associated objects that are clearly the F_0/F_1 ATP synthase [51]. Tomograms of liposomes filled with large protein complexes (proteasomes and thermosomes) have enabled such objects to be distinguished by 3D correlation analysis [60], although the ways in which a background of frozen cytosol will affect the recognition process remain to be determined. If the resolution of cryo-ET were improved to 2 or even 3 nm, the identification of many protein complexes without stains or labels should be possible [61,62].

Some protein complexes can be localized and identified in tomograms generated from RF-FSF samples. Microtubules are obvious, and even the γ-tubulin ring complex can be seen at the centrosome-proximal ends of many microtubules [3,4]; the size, shape and staining of the helical wrappings on membranous tubes in the phragmoplast resemble the dynamin polymers that form at necks of endocytic vesicles [12]. The reliable localization of diverse proteins in these samples, however, will require advances in techniques for tagging specific macromolecules with markers that are visible by EM.

Owing to their high affinity and specificity of binding, antibodies are powerful tools for protein localization and, coupled to electron-dense markers, they have long been used to identify antigens by EM of thin sections. However, only some antibodies work on well-fixed samples (in our laboratory, about 20 have worked out of 60 tried). In addition, antibodies cannot be easily delivered across the

membranes of living cells and their size, especially when coupled to electron-dense tags, inhibits their diffusion into the cytoplasm, even in the melted cryosections that are often used for immuno-EM [33]. The thick samples that take advantage of tomographic reconstruction are therefore particularly difficult specimens to label. Antibodies are widely used for light microscopy of comparatively thick samples because the fixations used for this method render cells highly permeable to antibody diffusion. These same fixations can, however, cause antigens to migrate [63]; in addition, they do not preserve the fine structure of a cell [64] and thus are not suitable for ET.

Concluding remarks and future perspectives

Published data show beyond doubt that ET can provide valuable views of cells and cell parts at resolutions that are useful for answering questions about cellular mechanisms. Cryo-ET of frozen-hydrated cells can be used to reconstruct samples whose preparation is so straightforward that the resulting image is highly likely to represent the living cell accurately. At present, however, this method is limited by the thickness of the samples that can be imaged, and this will continue to limit its influence on cell biology until techniques for cutting cryosections become easier to apply. Because cryo-Et also makes labeling difficult, the recognition of specific macromolecules will have to rely on the fidelity of preservation and the resolution of the images to identify molecules of interest.

If a resolution of 2–3 nm can be achieved, however, there will be strong motivation to devise efficient ways in which to compare the local structures in a tomogram with the atomic structures of macromolecular complexes, displayed at comparable resolution, such that the complexes can be localized in cells by cross-correlation of the images. Such improvements in resolution will require a significant increase in the amount and/or the effectiveness of the tolerable electron dose (Box 1).

Prospects for improving the resolution of ET

The resolution of ET is estimated to depend on dose as a one-third or one-fourth power [17,53], although this dependency will improve to a one-half to one-third power if thinner specimens can be used to seek higher resolution. Thus, obtaining a resolution of 2–3 nm with EM will require a 5–8-fold increase in the detected electron dose.

Box 1. Outstanding technical issues

- Increasing the electron dose that a cellular sample can tolerate
- Increasing the contrast in images of frozen-hydrated samples
- Cutting good cryo-sections, even serial sections, of frozen-hydrated samples
- Improving the ability of electronic cameras to capture energetic electrons (e.g. 300 keV) with better preservation of information about structural details (i.e. information at 'high spatial frequency')
- Developing automatic recognition of structural features in tomograms, both to trace the contours of cellular objects (e.g. membranes, chromatin and cytoskeletal fibers) and to identify particular macromolecular complexes
- Labeling specific macromolecules in well-fixed cells with tags that are readily visible in the EM

Some such improvements are bound to come from instrument technology. For example, the CCD cameras that are currently available have rather poor efficiency for detecting moderate-to-high resolution details with the 300-keV electrons that work well for thicker specimens. The devices that are currently being developed might increase this efficiency by a factor of 2 or more [65,66], enabling more-effective imaging without an increase in dose to the specimen. Imaging at lower temperatures (liquid helium) might improve the resistance of the specimen to beam damage [67], although an electron optical trick might be required to gain back the contrast that is lost at these temperatures. For example, a phase plate at the back focal plane of the objective lens, analogous to that used for phase-contrast light microscopy [68], might ultimately improve performance considerably.

Prospects for improving macromolecular labeling in ET

Effective methods for labeling macromolecular structures would constitute a major advance in cellular ET. An EM equivalent of the green fluorescent protein would be tremendously valuable, but such a reagent is hard to produce. Both the density and the size of a marker must be sufficient to enable its visualization against the background electron scattering from a specimen that is many nanometers thick. One or a few atoms of heavy metal will not work. Particles of gold with a diameter of about 1 nm ($\sim$20 atoms) can be seen with appropriate electron optics on 60-nm plastic sections [69], but when such samples are stained with heavy metals, the gold is hard to distinguish from the stain. Moreover, such discriminations require good counting statistics – that is, high electron doses – and are therefore unlikely to work on frozen-hydrated samples. Thus, a method that affixes a readily visible tag to its target during FSF would be a boon to cell biology.

Several groups are working to improve the EM tags for macromolecules. Progress has been made on the photoconversion of green fluorescent protein to an EM-visible marker [70]. Tsien's laboratory [71,72] has modified a fluorescent probe to make a small molecule that will diffuse into cells and bind covalently to four nearby sulfhydryl groups that are suitably arranged by protein secondary structure. After fixation, the dye can be made visible in the EM by the photo-induced oxidation of nearby diaminobenzidine, which produces an electron-visible precipitate near the site of the bound dye. Because the necessary array of cysteines can be engineered into most proteins of interest, this method should prove useful for the localization of many gene products.

Some groups are working to engineer metal-binding sites directly into their object of interest, for example, by making a chimera of a chosen protein and a metal-binding motif. Others are trying to identify a small label that will bind to a clonable tag that could be expressed as a fusion with the protein of interest [73]. Single-stranded oligonucleotides (aptamers) have some of the relevant properties: they are significantly smaller than antibodies, they bind to their targets with high affinity [74,75] and they are adequately soluble in cold acetone.

Target labeling for ET remains one of the foremost technical challenges that must be met to bring this method

to maximum use in cell biology. If these methods develop to the point at which we can map macromolecules into 3D cell structure, a new era in cell biology is bound to emerge.

Update

We would like to draw the readers' attention to a recently published article regarding the imaging of thicker freeze-substituted samples: Bouwer, J.C. *et al.* (2004) Automated most-probable loss tomography of thick selectively stained biological specimens with quantitative measurement of resolution improvement. *J. Struct. Biol.* 148, 297–306.

Acknowledgements

We thank E. O'Toole and A. Staehelin for criticism of the manuscript; K. Grunewald, M. Martone, M. Moritz, S. Nickell and M. Otegui for use of their micrographs; K. Christensen (Imagecyte) for providing bacteriophage cartoons; and the National Institutes of Health (GM 61306) and the National Center for Research Resources (RR 00592) for financial support.

Supplementary data

Supplementary data associated with this article can be found at doi:10.1016/j.tcb.2004.11.009

References

1 Frank, J. (1992) *Electron Tomography: Three Dimensional Imaging with the Transmission Electron Microscope*, Plenum Press
2 Koster, A.J. *et al.* (1997) Perspectives of molecular and cellular electron tomography. *J. Struct. Biol.* 120, 276–308
3 O'Toole, E.T. *et al.* (1999) High-voltage electron tomography of spindle pole bodies and early mitotic spindles in the yeast *Saccharomyces cerevisiae*. *Mol. Biol. Cell* 10, 2017–2031
4 O'Toole, E.T. *et al.* (2003) Morphologically distinct microtubule ends in the mitotic centrosome of *Caenorhabditis elegans*. *J. Cell Biol.* 163, 451–456
5 Baumeister, W. *et al.* (1999) Electron tomography of molecules and cells. *Trends Cell Biol.* 9, 81–85
6 O'Toole, E.T. *et al.* (2003) Three-dimensional organization of basal bodies from wild-type and δ-tubulin deletion strains of *Chlamydomonas reinhardtii*. *Mol. Biol. Cell* 14, 2999–3012
7 Moritz, M. *et al.* (2000) Structure of the γ-tubulin ring complex: a template for microtubule nucleation. *Nat. Cell Biol.* 2, 365–370
8 Frangakis, A.S. and Forster, F. (2004) Computational exploration of structural information from cryo-electron tomograms. *Curr. Opin. Struct. Biol.* 14, 325–331
9 Martone, M.E. *et al.* (2002) A cell-centered database for electron tomographic data. *J. Struct. Biol.* 138, 145–155
10 Volkmann, N. (2002) A novel three-dimensional variant of the watershed transform for segmentation of electron density maps. *J. Struct. Biol.* 138, 123–129
11 Otegui, M.S. *et al.* (2001) Three-dimensional analysis of syncytial-type cell plates during endosperm cellularization visualized by high resolution electron tomography. *Plant Cell* 13, 2033–2051
12 Segui-Simarro, J.M. *et al.* (2004) Electron tomographic analysis of somatic cell plate formation in meristematic cells of *Arabidopsis thaliana* preserved by high-pressure freezing. *Plant Cell* 16, 836–856
13 Olins, D.E. *et al.* (1983) Electron microscope tomography: transcription in three dimensions. *Science* 220, 498–500
14 Skoglund, U. *et al.* (1986) Three-dimensional structure of a specific pre-messenger RNP particle established by electron microscope tomography. *Nature* 319, 560–564
15 McEwen, B.F. *et al.* (1986) Tomographic three-dimensional reconstruction of cilia ultrastructure from thick sections. *Proc. Natl. Acad. Sci. U. S. A.* 83, 9040–9044
16 Belmont, A.S. *et al.* (1987) A three-dimensional approach to mitotic chromosome structure: evidence for a complex hierarchical organization. *J. Cell Biol.* 105, 77–92
17 Grimm, R. *et al.* (1998) Electron tomography of ice-embedded prokaryotic cells. *Biophys. J.* 74, 1031–1042
18 Ladinsky, M.S. *et al.* (1999) Golgi structure in three dimensions: functional insights from the normal rat kidney cell. *J. Cell Biol.* 144, 1135–1149
19 Escaig, J. (1982) New instruments which facilitate freezing at 83 K and 6 K. *J. Microsc.* 126, 221–229
20 McIntosh, J.R. (2001) Electron microscopy of cells: a new beginning for a new century. *J. Cell Biol.* 153, F25–F32
21 Dubochet, J. *et al.* (1988) Cryo-electron microscopy of vitrified specimens. *Q. Rev. Biophys.* 21, 129–228
22 Gilkey, J.C. and Staehelin, L.A. (1986) Advances in ultrarapid freezing for the preservation of cellular ultrastructure. *J. Electron Microsc. Tech.* 3, 177–210
23 Dubochet, J. *et al.* (1983) Electron microscopy of frozen-hydrated bacteria. *J. Bacteriol.* 155, 381–390
24 Hunziker, E.B. *et al.* (1984) Cartilage ultrastructure after high pressure freezing, freeze substitution, and low temperature embedding. I. Chondrocyte ultrastructure – implications for the theories of mineralization and vascular invasion. *J. Cell Biol.* 98, 267–276
25 Dahl, R. and Staehelin, L.A. (1989) High pressure freezing for the preservation of biological structure: theory and practice. *J. Electron Microsc. Tech.* 13, 165–174
26 Studer, D. *et al.* (1989) High pressure freezing comes of age. *Scanning Microsc.* 3, 253–269
27 Sartori, N. *et al.* (1993) Vitrification depth can be increased more than 10-fold by high-pressure freezing. *J. Microsc.* 172, 55–61
28 Vanhecke, D. *et al.* (2003) A rapid microbiopsy system to improve the preservation of biological samples prior to high-pressure freezing. *J. Microsc.* 212, 3–12
29 O'Toole, E.T. *et al.* (2002) Electron tomography of yeast cells. *Methods Enzymol.* 351, 81–95
30 McDonald, K. and Morphew, M.K. (1993) Improved preservation of ultrastructure in difficult-to-fix organisms by high pressure freezing and freeze substitution: I. *Drosophila melanogaster* and *Strongylocentrotus purpuratus* embryos. *Microsc. Res. Tech.* 24, 465–473
31 Kiss, J.Z. and Staehelin, L.A. (1995) High pressure freezing. In *Rapid Freezing, Freeze Fracture, and Deep Etching* (Severs, N.J. and Shotton, D.M., eds), pp. 89–104, Wiley-Liss
32 Zalokar, M. (1966) A simple freeze-substitution method for electron microscopy. *J. Ultrastruct. Res.* 15, 469–479
33 Steinbrecht, R.A. and Muller, M. (1987) Freeze-substitution and freeze drying. In *Cryotechniques in Biological Electron Microscopy* (Steinbrecht, R.A. and Zierold, K., eds), pp. 149–172, Springer-Verlag
34 Linder, J.C. and Staehelin, L.A. (1979) A novel model for fluid secretion by the trypanosomatid contractile vacuole apparatus. *J. Cell Biol.* 83, 371–382
35 Kellenberger, E. (1991) The potential of cryofixation and freeze substitution: observations and theoretical considerations. *J. Microsc.* 161, 183–203
36 Sosa, H. *et al.* (1994) Ultrastructure of skeletal muscle fibers studied by a plunge quick freezing method: myofilament lengths. *Biophys. J.* 67, 283–292
37 Marsh, B.J. *et al.* (2001) Organellar relationships in the Golgi region of the pancreatic β cell line, HIT-T15, visualized by high resolution electron tomography. *Proc. Natl. Acad. Sci. U. S. A.* 98, 2399–2406
38 Crowther, R.A. *et al.* (1970) Three dimensional reconstructions of spherical viruses by Fourier synthesis from electron micrographs. *Nature* 226, 421–425
39 Radermacher, M. (1992) Weighted back projection methods. In *Electron Tomography: Three Dimensional Imaging with the Transmission Electron Microscope* (Frank, J., ed.), pp. 91–115, Plenum Press
40 Penczek, P. *et al.* (1995) Double-tilt electron tomography. *Ultramicroscopy* 60, 393–410
41 Mastronarde, D.N. (1997) Dual-axis tomography: an approach with alignment methods that preserve resolution. *J. Struct. Biol.* 120, 343–352
42 McEwen, B.F. *et al.* (1995) The relevance of dose-fractionation in tomography of radiation-sensitive specimens. *Ultramicroscopy* 60, 357–373
43 He, W. *et al.* (2003) Untangling desmosomal knots with electron tomography. *Science* 302, 109–113
44 Luther, P.K. *et al.* (1988) A method for monitoring the collapse of plastic sections as a function of electron dose. *Ultramicroscopy* 24, 7–18

45 Al-Amoudi, A. *et al*. (2004) Cryo-electron microscopy of vitreous sections of native biological cells and tissues. *J. Struct. Biol.* 148, 131–135
46 Taylor, K.A. and Glaeser, R.M. (1976) Electron microscopy of frozen hydrated biological specimens. *J. Ultrastruct. Res.* 55, 448–456
47 Hayward, S.B. and Glaeser, R.M. (1979) Radiation damage of purple membrane at low temperature. *Ultramicroscopy* 4, 201–210
48 Leapman, R.D. and Sun, S. (1995) Cryo-electron energy loss spectroscopy: observations on vitrified hydrated specimens and radiation damage. *Ultramicroscopy* 59, 71–79
49 Nickell, S. *et al*. (2003) *Pyrodictium cannulae* enter the periplasmic space but do not enter the cytoplasm, as revealed by cryo-electron tomography. *J. Struct. Biol.* 141, 34–42
50 Medalia, O. *et al*. (2002) Macromolecular architecture in eukaryotic cells visualized by cryoelectron tomography. *Science* 298, 1209–1213
51 Nicastro, D. *et al*. (2000) Cryo-electron tomography of neurospora mitochondria. *J. Struct. Biol.* 129, 48–56
52 Mannella, C.A. *et al*. (2001) Topology of the mitochondrial inner membrane: dynamics and bioenergetic implications. *IUBMB Life* 52, 93–100
53 McEwen, B.F. *et al*. (2002) Use of frozen-hydrated axonemes to assess imaging parameters and resolution limits in cryoelectron tomography. *J. Struct. Biol.* 138, 47–57
54 McDowell, A. *et al*. (1989) The structure of organelles of the endocytic pathway in hydrated cryosections of cultured cells. *Eur. J. Cell Biol.* 49, 289–294
55 Hsieh, C.E. *et al*. (2002) Electron tomographic analysis of frozen-hydrated tissue sections. *J. Struct. Biol.* 138, 63–73
56 Matias, V.R. *et al*. (2003) Cryo-transmission electron microscopy of frozen-hydrated sections of *Escherichia coli* and *Pseudomonas aeruginosa*. *J. Bacteriol.* 185, 6112–6118
57 Tokuyasu, K.T. (1980) Immunochemistry on ultrathin frozen sections. *Histochem. J.* 12, 381–403
58 Grunewald, K. *et al*. (2003) Three-dimensional structure of herpes simplex virus from cryo-electron tomography. *Science* 302, 1396–1398
59 Walz, J. *et al*. (1997) Electron tomography of single ice-embedded macromolecules: three-dimensional alignment and classification. *J. Struct. Biol.* 120, 387–395
60 Frangakis, A.S. *et al*. (2002) Identification of macromolecular complexes in cryoelectron tomograms of phantom cells. *Proc. Natl. Acad. Sci. U. S. A.* 99, 14153–14158
61 Baumeister, W. (2002) Electron tomography: towards visualizing the molecular organization of the cytoplasm. *Curr. Opin. Struct. Biol.* 12, 679–684
62 Grunewald, K. *et al*. (2003) Prospects of electron cryotomography to visualize macromolecular complexes inside cellular compartments: implications of crowding. *Biophys. Chem.* 100, 577–591
63 Melan, M.S. and Sluder, G. (1992) Redistribution and differential extraction of soluble proteins in permeabilized cell cultures: implications for immunofluorescence microscopy. *J. Cell Sci.* 101, 731–743
64 McDonald, K.L. (1994) Electron microscopy and EM immunocytochemistry. *Methods Cell Biol.* 44, 411–444
65 Downing, K.H. *et al*. (2000) Electron decelerator for improved CCD performance in intermediate voltage electron microscopy. *Microsc. Microanal.* 6 (Suppl. 2), 734–735
66 Bailey, B. *et al*. (2004) Performance evaluation of a transmission scintillator-based lens-coupled 4K CCD camera for use in low-dose electron cryo-tomography. *Microsc. Microanal.* 10 (Suppl. 1), 90
67 Chiu, W. *et al*. (1986) Cryoprotection in electron microscopy. *J. Microsc.* 141, 385–391
68 Danev, R. and Nagayama, K. (2001) Transmission electron microscopy with Zernike phase plate. *Ultramicroscopy* 88, 243–252
69 Ziese, U. *et al*. (2002) Three-dimensional localization of ultrasmall immuno-gold labels by HAADF-STEM tomography. *J. Struct. Biol.* 138, 58–62
70 Grabenbauer, M. (2003) Photoconversion of the green fluorescent protein. *Mol. Biol. Cell* 14, 104a
71 Gaietta, G. *et al*. (2002) Multicolor and electron microscopic imaging of connexin trafficking. *Science* 296, 503–507
72 Ju, W. *et al*. (2004) Activity-dependent regulation of dendritic synthesis and trafficking of AMPA receptors. *Nat. Neurosci.* 7, 244–253
73 Stanlis, K.K. and McIntosh, J.R. (2003) Single-strand DNA aptamers as probes for protein localization in cells. *J. Histochem. Cytochem.* 51, 797–808
74 Bianchini, M. *et al*. (2001) Specific oligobodies against ERK-2 that recognize both the native and the denatured state of the protein. *J. Immunol. Methods* 252, 191–197
75 Blank, M. *et al*. (2001) Systematic evolution of a DNA aptamer binding to rat brain tumor microvessels. selective targeting of endothelial regulatory protein pigpen. *J. Biol. Chem.* 276, 16464–16468